Journal of Chromatography A 1694 (2023) 463922

Contents lists available at ScienceDirect

Journal of Chromatography A

journal homepage: www.elsevier.com/locate/chroma

A monolithic composite based on zeolite-like metal-organic framework@divinylbenzene polymer separates azeotropic fluorocarbon mixture efficiently

Kareem Yusuf[a,*], Osama Shekhah[b], Ahmad Aqel[a], Seetah Alharbi[a], Ali S. Alghamdi[a], Reem M. Aljohani[a], Mohamed Eddaoudi[b], Zeid A. ALOthman[a]

[a] Department of Chemistry, College of Science, King Saud University, P.O. Box 2455, Riyadh 11451, Saudi Arabia
[b] Functional Materials Design, Discovery and Development Research Group (FMD3), Advanced Membranes and Porous Materials Centre (AMPMC), Physical Sciences and Engineering Division, King Abdullah University of Science and Technology (KAUST), P.O. Box 6900, Jeddah 23955, Saudi Arabia

ARTICLE INFO

Article history:
Received 5 January 2023
Revised 4 March 2023
Accepted 7 March 2023
Available online 12 March 2023

Keywords:
Monolith
Metal-organic frameworks
Gas chromatography
Fluorocarbon
Global warming

ABSTRACT

Organic monolithic columns are mainly used to separate macromolecules; however, many attempts to extend their performance toward small molecules were examined by incorporating micro- and nanoparticles. The incorporation technique enabled utilizing organic monoliths in gas chromatography (GC) for small molecules, which are still scarce. Here, we prepared a composite matrix of capillary monolithic columns of a zeolite-like metal-organic framework with a sodalite topology (sod-ZMOF) and Divinylbenzene polymer (DVB) for GC separations under 0.5 MPa. Relatively short DVB monolithic columns (18 cm long × 0.25 mm i.d.) incorporated with a tiny amount of sod-ZMOF nanoparticles (0.7 and 1.17 wt%) with an average particle size of 225 nm were successfully fabricated and used to separate linear alkanes and polar probes mixtures with increasing resolution up to 3.7 and 5.1 times, respectively, compared to a blank DVB monolithic column. A high-performance separation of linear alkanes series mixture (methane to decane) was exhibited in less than 2 min. McReynolds constants revealed that sod-ZMOF provided the composite monolith with a nonpolar character yielding a negative average polarity value smaller than the standard squalene column. An Excellent retention time of pentane and octane day-to-day reproducibility was achieved during 16 days and over more than 500 runs with RSD% of 2.25% and 3.3% using a composite monolithic column with 5 mg mL^{-1} sod-ZMOF (5-ZMOF@DVB). In addition, a qualitative determination of the gas mixture content of three commercially available Lighter gas cartridges was performed via the 5-ZMOF@DVB column. Finally, successfully separating an azeotropic freon mixture of difluoromethane (R-32) and pentafluoroethane (R-125) was achieved with a selectivity of up to 4.84. A further thermodynamic study related the preferential adsorption of R-125 to entropic factors rather than enthalpic while trapping inside ZMOF pores. This work sheds light on utilizing the infinite diversity of MOFs and combining their properties with high permeability and easily fabricated organic monoliths for GC separations of light molecules and gasses. Furthermore, the study highlights the role of GC as an easy and fast approach for the preliminary evaluation of the separation efficiency of porous polymers.

1. Introduction

Metal-organic frameworks (MOFs) are crystalline porous materials with infinite structure diversity due to extreme structural component variability [1,2]. MOFs consist of an inorganic part (i.e. metal ions or clusters) and organic ligand to form well-defined crystals that found their place in several applications, especially separation applications, due to their high surface area, superior stability, tunable chemical nature, designable porous structure, and high thermal stability [3–7]. Therefore, there are many attempts to use MOFs as a stationary phase in GC in various forms such as packed columns, open-tubular columns [8,9], and incorporated into a monolithic matrix [10].

Monoliths are a single continuous sponge-like material with a bimodal porous structure [11]. Macropores (1.5–4 μm) guarantee high permeability of the mobile phase, and micropores (10–20 nm) provide the matrix with a unique separation ability regarding its chemical nature [12]. Monolithic columns are found in two primary forms, organic monoliths (polymer-based), which

* Corresponding author.
E-mail address: kmahmoud@ksu.edu.sa (K. Yusuf).

https://doi.org/10.1016/j.chroma.2023.463922
0021-9673/

are more suitable for macromolecules separation such as proteins and polysaccharides, and inorganic monoliths (silica-based), which are convenient for small molecules separation [13]. Easy fabrication and diverse chemistries are the main advantages of organic over inorganic monoliths, while the significant disadvantage is the limited applicability with small molecules. Therefore, incorporating various micro- and nanoparticles, including MOFs, into monolithic organic columns is a common practice to extend their separation efficiency towards small molecules [14]. MOF@monolith composite would combine the properties of MOFs, for instance, high surface area, designable structure and the probability of post-synthetic modification, and the high permeability of monoliths.

While monolithic columns are widely used in LC, they are still scarce in GC applications [8,9]. The reason behind the minimal studies of monoliths in GC is the need for a modified gas chromatograph to afford the suitable high pressure (up to 10 MPa, which is ten times higher than conventional GC pressure) to overcome monolithic matrix back pressure [15]. Divinylbenzene copolymerized with styrene was used two decades ago in the first attempt to use monolithic columns in GC [16], and since this pioneering work, very few studies have examined the performance of monolithic columns in GC. Kurganov's group has impressive work on GC monolithic column applications [15]; however, the use of a modified high-pressure gas chromatograph in this work limit a wider adoptability of such a technique. Another interesting research used DVB-based monoliths as a second-dimension column in a conventional GC [17]. Methacrylate-based monoliths are also utilized in GC [10]. Our research group had several endeavors to develop different types of methacrylate monoliths for GC applications, whether neat methacrylates [18] or incorporated with various particles [19–22]. Fabricating a composite ZIF-8@methacrylate GC monolithic column was the first and only attempt to incorporate MOF microparticles into a monolithic matrix for conventional gas chromatograph [19], followed by an inverse gas chromatography study of the same stationary phase for a deeper understanding of its separation ability in terms of physicochemical properties of adsorption [20]. The addition of ZIF-8 into the methacrylate monolith increased the BET surface area up to 3.4 times and elevated efficiency 4–5 times compared to the blank methacrylate monolith. The low thermal stability of methacrylate monoliths (about 190 °C) and poor dispersion of ZIF-8 microparticles were the major disadvantages of ZIF-8@methacrylate monolithic material.

Zeolite-like MOFs (ZMOFs) are considered as a subclass of MOFs that mimic the structural and, in some cases, functional features of traditional inorganic zeolites [23]. The interest in ZMOFs stems from the remarkable industrial virtue of zeolites, especially in adsorption, ion exchange, and catalysis [24–26]. The design approach to construct ZMOFs is simply based on replacing an oxygen atom with an organic moiety with embedded angular connectivity equivalent to that of zeolites, which is referred to as "edge expansion" [23]. The N-heterocyclic compounds like for example imidazole, triazole, and tetrazole, meet the coordination directionality criterion of organic ligands for ZMOF formation synthesis and many successful examples have been reported for the synthesis of ZMOFs with 4- and 6- or 8- coordinated metals by Eddaoudi's group [23]. The N- atoms in the aromatic ring of the ligand provide binding directionality, while the O- from carboxylic acids lock the metals in place, resulting in geometrically rigid anionic MBBs.

The Indium-based sod-ZMOF is used in a membrane form as a molecular sieve to separate various gas binary mixtures such as CO_2/CH_4, CO_2/O_2, CO_2/N_2, and CO_2/H_2 [27]. Remarkably, it showed a selective permeability toward CO_2 in all cases due to its anionic character and relatively small and rigid pore aperture (4.1 Å). Furthermore, utilizing sod-ZMOF incorporated into a polyimide matrix as a mixed-matrix membrane even increased its permeability of CO_2 [28,29]. Monte Carlo simulations of the propane/propylene separation performance of sod-ZMOF successfully confirmed the effect of ZMOFs anionic framework in the selective adsorption efficiency in favor of the higher dipole moment propylene [30]. Recently, molecular sieving-based separation of butane/isobutene mixture was reported using a ZMOF-based membrane [31]. Despite a few studies investigating the separation performance of light hydrocarbons of different ZMOF topologies (rho-ZMOF and ana-ZMOF) via breakthrough experiments [32,33], to the best of our knowledge, sod-ZMOF was not examined for light hydrocarbons separation. It is worth noting that chromatographic studies show the separation performance for a multicomponent mixture of the tested stationary phase utilizing microgram quantity, while breakthrough experiments need about 200 mg at least for a precise separation behavior examination with a lot of technical difficulties for multicomponent mixtures [34].

In this work, sod-ZMOF nanoparticles were prepared and incorporated into a highly permeable macroporous DVB monolithic matrix to enhance its separation ability toward gasses and small nonpolar and polar molecules. The composite monolithic matrix was prepared in the form of short capillary columns (18 cm × 250 µm i.d) with different percentages of sod-ZMOF. The fabricated columns were used to separate different mixtures of gasses, linear alkanes, aromatics, cycloalkanes, and polar probes under a relatively low pressure (0.5 MPa) using a conventional gas chromatograph. In addition, the prepared columns' chromatographic performance, efficiency, and polarity were investigated to evaluate the effect of sod-ZMOF incorporation. Finally, the prepared ZMOF@DVB composite monoliths were successfully utilized to separate an azeotropic fluorocarbon mixture of difluoromethane (R-32) and pentafluoroethane (R-125), which is one of the major consumed refrigerants for air-conditioners and heat pumps under the commercial code R-410A.

2. Experimental section

2.1. Chemicals and materials

Indium (III) nitrate hydrate, 4,5-Imidazoledicarboxylaic acid (4,5-ImDC), PVP30, dimethylformamide (DMF), imidazole, and divinylbenzene (DVB) monomers were obtained from Sigma-Aldrich (St. Louis, MO, USA). Fused silica capillaries (250 µm i.d.) were purchased from CM Scientific Ltd (Bradford, UK). Azobisisobvutyronitrile (AIBN) and 3-(trimethoxysilyl) propyl methacrylate (TMSM) were purchased from Fluka (Buchs, Switzerland). High-purity grade (99.9999%) gasses (methane, ethane, propane, butane, helium, hydrogen, nitrogen, and air) were purchased from SIGAS (Riyadh, Saudi Arabia). Linear alkanes (Pentane, hexane, heptane, octane, nonane, and decane) in addition to cyclopentane, acetonitrile (ACN), diethyl ether (DEE), tetrahydrofuran (THF), ethyl acetate (EA) 1-dodecanol, and methanol were obtained from Merck (Darmstadt, Germany). Benzene, toluene, ethylbenzene, cyclohexane, acetone (AC), pyridine (PY), 1-butanol, 2-pentanone, and 1-nitropropane were purchased from BDH (Lutterworth, UK). R-410A was purchased from Honeywell International Inc. (North Carolina, US). All chemicals were used without further purification.

2.2. Instrumentation

PXRD patterns were performed on a D8 Advance X-ray diffractometer (Bruker, Germany) with a Cu K-alpha radiation (λ=1.5406 Å). Argon adsorption-desorption isotherms were completed using 3-Flex Surface Characterization Analyzer with enhanced corrosion resistance (ECR) from Micromeritics. TA Instruments hi-res TGA Q500 thermogravimetric analyzer was used for thermogravimetric analysis (TGA) under a continuous N_2 flow and at a heating rate of 5 °C per minute. Low-pressure gas sorption

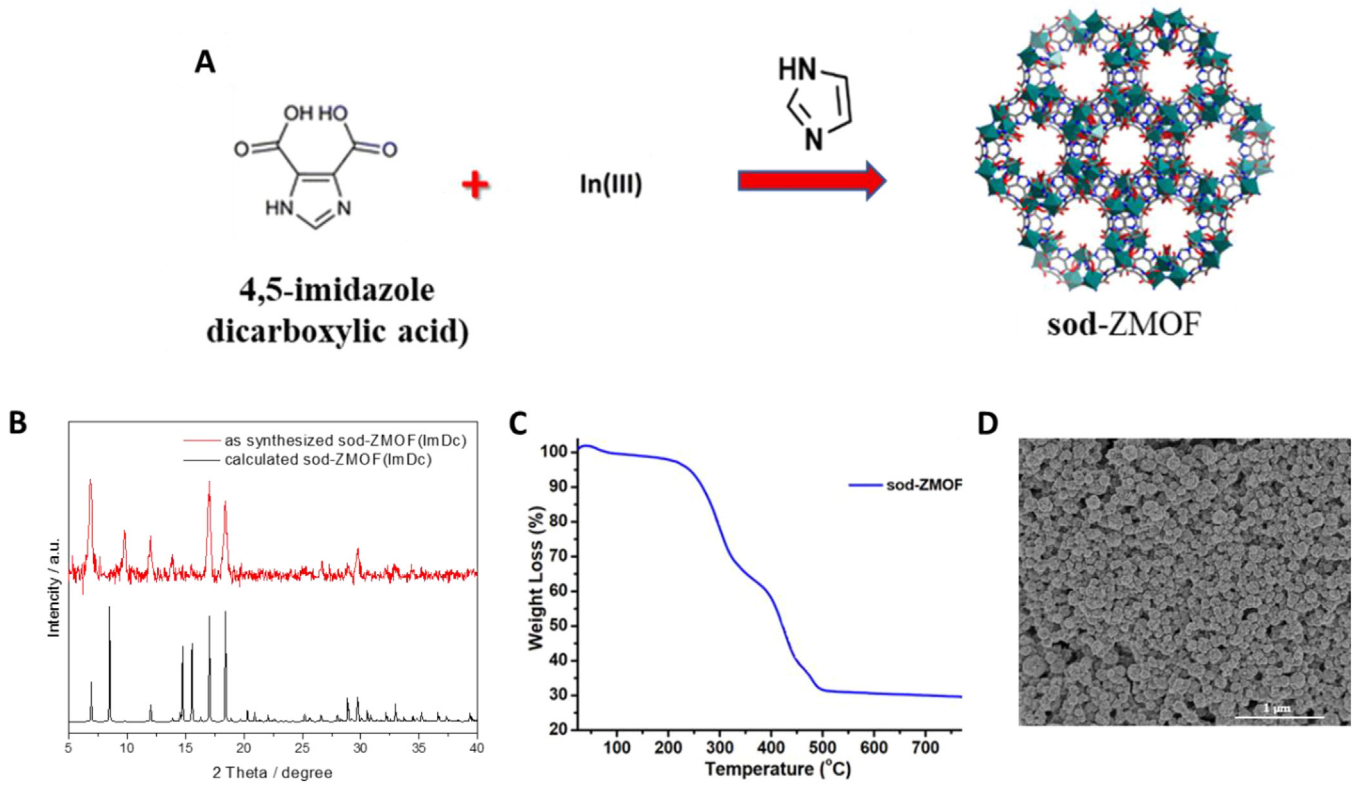

Fig. 1. (A) Schematic for the synthesis of sod-ZMOF, (B) PXRD patterns of sod-ZMOF: simulated (black) and as-synthesized (red), (C) Thermogravimetric curve of sod-ZMOF, and (D), SEM images of sod-ZMOF.

measurements were performed on a fully automated Autosorb-IQ gas sorption analyzer (Quantachrome Instruments). SEM images were obtained with a Zeiss DSM 950 scanning electron microscope and FEI, QUANTA 200 3D Scanning Electron Microscope with tungsten filament as electron source operated at 10 kV.

All chromatographic experiments were performed using a Shimadzu 2025 Series conventional gas chromatograph. The system is equipped with a split/splitless injection unit (SPL), an oven with a temperature range from room temperature +10 to 400 °C and 14.5 °C s^{-1} heating rate, and a flame ionization detector (FID) with a 1:10 (hydrogen: air) fuel mixture. The bulk temperature of the injector and detector was adjusted to 250 °C, and samples were introduced by manual injection. A dried high-purity helium was utilized as the carrier gas.

2.3. sod-ZMOF nanoparticles preparation

15 mg of $In(NO_3)_3.\ 2H_2O$ dissolved in 1 ml of DMF, 15 mg of 4,5-ImDC dissolved in acetonitrile, 0.2 ml of 1.47 M imidazole solution in DMF, and 0.5 ml of 0.01 M of PVP30 in DMF were mixed in a 20 ml sonication vial. The mixture was heated under 85 °C with stirring for 24 h. The product was washed extensively with DMF 3 times, and then it was solvent exchanged with methanol every 12 h for 2 days (Fig. 1A).

2.4. Monolithic columns preparation

The preparation procedure of monolithic columns was chosen to provide the monolithic structure with relatively large pores and high permeability, and thus can work under low gas pressure, according to a previously described method [35]. Briefly, the monoliths are covalently immobilized to the inner walls of the empty capillary. Therefore, before polymerization, a surface pretreatment of the fused silica capillaries' inner wall was performed. A 5 m long empty tubing (250 µm i.d) was rinsed with 1.0 mol L^{-1} NaOH solution for 30 min and then washed with distilled water for another 30 min. The previous step was repeated by replacing sodium hydroxide with 0.2 mol L^{-1} HCl and washing with acetone for 5 min after water, then drying under a nitrogen stream for 2 h. The column was then filled with 40 wt.% 3-(trimethoxysilyl) propyl methacrylate (TMSM) solution in acetone and stood for 2 h, then washed with acetone and dried again for 2 h with nitrogen. All flushing steps were performed at a flow rate of 20 µL min^{-1} using a syringe pump. The polymerization mixture consisted of a single monomer of DVB (42.3 wt%) and 57.7 wt% of a binary porogenic mixture (52.3 wt% 1-dodecanol and 5.4 wt% toluene), in addition to 1 wt% AIBN with respect to the monomer as an initiator.

Next, the polymerization mixture was sonicated for 10 min and purged with helium for 10 min. Afterward, each column was adjusted to 30 cm total length with 18 cm filled with polymerization mixture, which is localized in the middle of the tubing by hanging the column in a U-shape to avoid the continuous exposure of monoliths to inlet and outlet constant temperature of 250 °C at both ends of the column. Finally, thermal polymerization was carried out inside the GC oven under 73 °C for 30 min after filling the pretreated capillary tubing with polymerization mixture and sealing it with GC septa. The remaining mixture in the vial was also polymerized under the same conditions as a bulk sample for further characterization.

Three column batches were prepared to study the effect of incorporating **sod**-ZMOF nanoparticles into the monolithic matrix, neat-DVB (without any **sod**-ZMOF), 3-ZMOF@DVB (3 mg mL^{-1} **sod**-ZMOF), and 5-ZMOF@DVB (5 mg mL^{-1} **sod**-ZMOF) account for 0, 7.7, and 12.8 μg of **sod**-ZMOF, respectively, regarding a total weight of 1.1 mg composite in each column. After polymerization, columns were flushed overnight with methanol using HPLC to remove the unreacted materials and porogenic solvents. Simultaneously, the bulk samples were washed with methanol overnight using Soxh-

let extraction and dried in a vacuum oven at 60 °C for 2 h before being used for characterization. Before use, the monolithic columns were conditioned using GC at a constant temperature of 40 °C and increasing pressure gradually with a rate of 0.01 MPa min^{-1} up to 1 MPa. Then, further conditioning was carried out under constant pressure of 0.5 MPa and a temperature program starting with 40 °C for 10 min, then ramp to 250 °C at a ramp rate of 3 °C min^{-1}, and finally, 250 °C for 30 min. The temperature program was repeated two times.

2.5. Chromatographic conditions and calculations

18 cm composite stationary phases were configured in the middle of 30 cm capillary tubing before polymerization to ensure isothermal conditions throughout the monolithic bed. This setup has the additional advantage of allowing the use of very short columns. Flow rates (F_a) were measured using a soap bubble method via a calibrated 100 µL glass pipette. Methane gas as unretained material was utilized to determine the dead time (t_0) under working conditions. The separation performance of the prepared ZMOF@DVB monolithic columns was evaluated through the separation of various mixtures of linear alkane gasses (methane, ethane, propane, and butane) and liquids (pentane, hexane, heptane, octane, nonane, and decane), cycloalkanes (cyclopentane, and cyclohexane), aromatics (benzene, toluene, and ethyl benzene), and polar probes (acetonitrile (ACN), acetone (AC), diethylether (DEE), tetrahydrofuran (THF), ethyl acetate (EA), and pyridine (PY)). All chromatographic experiments were injected in triplicate via a 5 μL syringe manual injection, while a gas-tight syringe was used for gas samples.

Permeability (K^o) of the monolithic columns was calculated using the modified Darcy's equation [8]:

$$K^{\circ} = \frac{u\eta L}{\Delta P\ j'} \tag{1}$$

Where u and η are the carrier gas (helium) velocity and viscosity, respectively, L is the column length, $\Delta P = P_i - P_o$ (as P_i is the column inlet pressure and P_o is the column outlet pressure of the carrier gas), and j' is the Halasz compressibility correlation factor ($j' = 3(P^2-1)(P+1)/4(P^3-1)$), where P equals P_i/P_o.

Hagen–Poiseuille equation was utilized to determine the average diameter of the monolithic channels (R) [36]:

$$u = \frac{\Delta P R^2}{8\eta L} \tag{2}$$

The selectivity (α) was determined as the ratio of the reduced retention times.

$$\alpha = \frac{t_{R2} - t_o}{t_{R1} - t_o} \tag{3}$$

While resolution (R_S) was calculated using the average width of peaks at half height ($w_{0.5}$) according to the following equation:

$$R_S = 1.18\ \frac{t_{R2} - t_{R1}}{w_{(0.5)1} + w_{(0.5)2}} \tag{4}$$

McReynolds constants were calculated under a working temperature of 100 °C for the neat-DVB columns. In contrast, for the composite columns, the working temperature was 180 °C to avoid miscalculations due to asymmetrical peaks that appear at a lower temperature for composites and to avoid peaks overlapping at higher temperatures for the neat-polymer columns.

2.6. Thermodynamic calculations

The retention volume (V_N) was the primary figure to calculate all thermodynamic parameters [37]:

$$V_N = (t_R - t_0)F_a\ \frac{T}{Ta} j \tag{5}$$

Where T is the working temperature, T_a is the ambient temperature, and j represents the gas compressibility factor of James-Martin and determined from the following equation [38]:

$$j = \frac{3\left(P^2 - 1\right)}{2\left(P^3 - 1\right)} \tag{6}$$

Henry constant (K) as the analog of the linear isotherm's slope was calculated as follows [39,40].

$$K = \frac{V_N}{R\ T} \tag{7}$$

The enthalpy change of adsorption (ΔH_A) represented the adsorbate-adsorbent degree of interaction at zero surface coverage. It was estimated by plotting the logarithm of V_N obtained from isothermal GC measurements vs. the inverse of absolute temperature [39].

$$\Delta H_A = -R\frac{d \ln\ V_N}{d\ (1/T)} \tag{8}$$

The Gibbs free energy change of adsorption (ΔG_A) is also calculated from the retention volume via Eq. (9) [37]:

$$\Delta G_A = -RTln\left(\frac{V_N\ P^o}{m\ S\ \pi 0}\right) \tag{9}$$

Where m is the mass of the stationary phase, π_0 is the reference two-dimensional surface pressure, S is the adsorbent's specific surface area, and P° is the vapor pressure of the adsorbate molecules, which was determined from Antoine's equation:

$$Log(P^{\circ}) = A - \left(\frac{B}{t + c}\right) \tag{10}$$

Where t is the temperature in degrees Celsius, and A, B, and C represent the Antoine coefficients.

Entropy change of adsorption (ΔS_A) is then calculated from ΔG_A and ΔH_A using the following equation [39]:

$$\Delta S_A = \frac{\Delta H_A - \Delta G_A}{T} \tag{11}$$

3. Results and discussion

3.1. Characterization of sod-ZMOF and ZMOF@DVB monolithic columns

The phase purity of the synthesized sod-ZMOF was confirmed by PXRD characterization. Furthermore, the pattern comparison of as-synthesized sod-ZMOF with the calculated sod-ZMOF pattern (Fig. 1B) is in perfect agreement. Thermal stability is a critical issue when it comes to GC applications. TGA results show excellent thermal stability for sod-ZMOF up to 250 °C (Fig. 1C). The SEM images of the prepared sod-ZMOF showed the synthesis of homogeneous nanoparticles with a size of about 200 nm with no aggregates (Fig. 1D).

The single gas equilibrium adsorption isotherm for CO_2 was also measured at 25 °C, which exhibited a typical type 1 isotherm. No significant difference was observed in gas uptake or enthalpy of adsorption for CO_2, compared for pristine material compared to previously reported materials (Fig. S2) [23]. Incorporating a tiny amount of sod-ZMOF into a 3-ZMOF@DVB monolithic composite (0.7 wt%) led to a significant increase of the BET surface area of the neat DVB monolith from 99.24 g m^{-2} to 116.75 g m^{-2}, and the surface area almost doubled (183.61 g m^{-2}) when adding 1.17 wt% of sod-ZMOF in the 5-ZMOF@DVB monolithic composite.

SEM results of the neat-DVB monolith showed well-developed spherical microglobules with a diameter range of 1–2 µm clustered around relatively large macropores with an average diame-

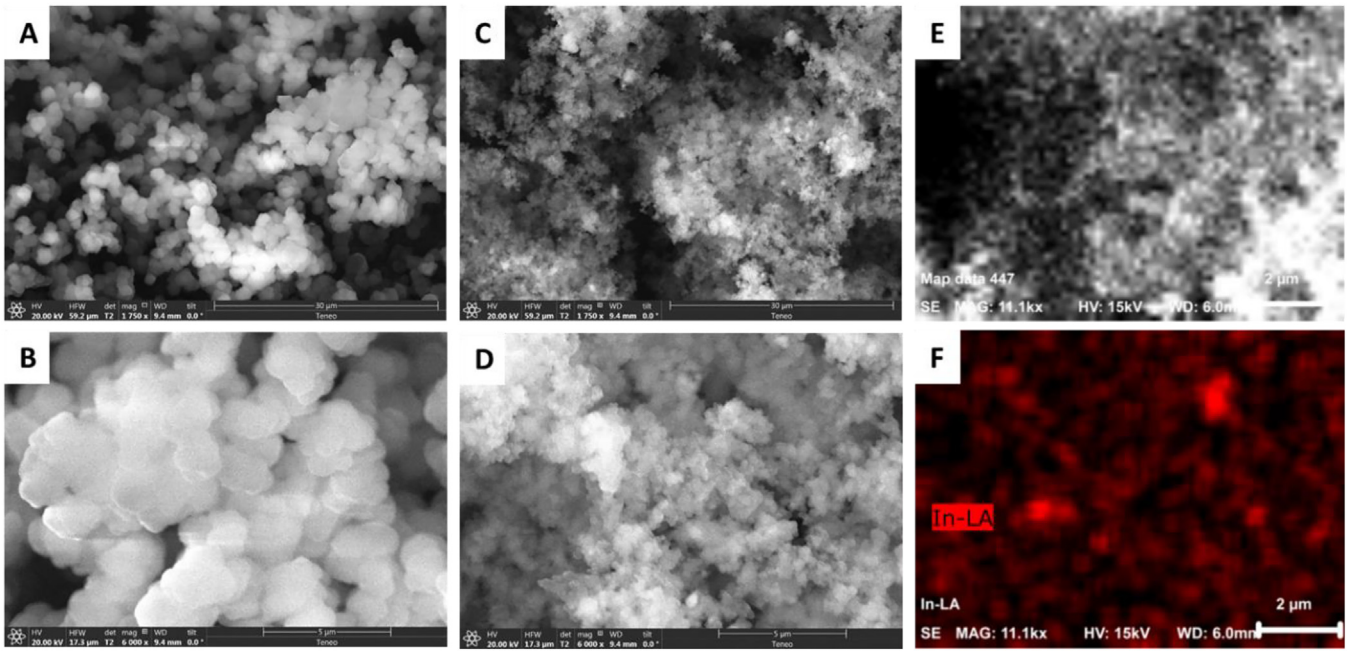

Fig. 2. Characterization of monolithic columns. (A, B) SEM images of neat-DVB monolithic composite. (C, D, and E) SEM images of 5-ZMOF@DVB monolithic composite. (F) Energy dispersive X-ray spectroscopy (EDS) element mapping image of 5-ZMOF@DVB monolithic composite shown in E.

ter of 5–10 μm (Fig. 2A and B). In contrast, the monolith's microglobuler structure was deformed by the effect of adding sod-ZMOF nanoparticles to form smaller clusters (Fig. 2C and D). The impact of sod-ZMOF on the monolithic structure and the higher percentage of micropores brought by the porous nanoparticles has led to a decreasing average pore size with increasing sod-ZMOF percentage. As a result, the average pore size reduced from 7.99 μm in the neat-DVB monolith to 6.28 and 5.58 μm in 3-ZMOF@DVB and 5-ZMOF@DVB monolithic composite, respectively. Similarly, the permeability calculations according to the modified Darcy Law (Eq. (1)) of the studied monoliths decreased in 3-ZMOF@DVB monolithic composite to about two-thirds its value (6.44×10^{-12} m^2) and in 5-ZMOF@DVB monolithic composite to about half its value (5.09×10^{-12} m^2) compared with the neat monolith permeability (10.40×10^{-12} m^2).

The nano-size homogenous structure of sod-ZMOF has led to a uniform distribution of the composite polymerization mixture. Furthermore, energy Dispersive x-ray Spectroscopy (EDS) element mapping image confirmed the homogeneity of the composite monolith by detecting the distribution of indium atoms within ZMOF structure in 5-ZMOF@DVB monolithic composite after polymerization (Figs. 2E, F, S3, and S4).

3.2. Polarity study

McReynolds constants approach is the most proper technique to evaluate the polarity nature of stationary phases using a number of probes, as each probe represents a specific type of interaction [41,42]. Pyridine, 1-butanol, benzene, 2-pentanone, and 1-nitropropane were used to determine McReynold constants for neat-DVB monolith compared to the composite monolithic materials. Consistent with previous studies on DVB as a polymer and on its monolithic form [43], neat-DVB monolith showed a nonpolar nature, which is even lower than the commercial stationary phase HP-5MS and single-wall carbon nanotubes (SWNT) (Table 1) [44,45]. Surprisingly, sod-ZMOF provided the composite monolith with a more nonpolar character yielding a negative average polarity value smaller than the standard squalene column. Despite the small amount of sod-ZMOF within the composite matrix (0.7 wt.% in 3-ZMOF@DVBm and 1.17 wt.% in 5-ZMOF@DVB), it has a significant effect on polarity, and as the nanoparticles percentage increases as the polarity significantly decrease.

Table 1
McReynolds constants for ΔI neat-DVB, 3-ZMOF@DVB, and 5-ZMOF@DVB compared to values for similar materials reported in the literature.

Stationary phase	X'	Y'	Z'	U'	S'	Average
ΔI Squalane	0	0	0	0	0	**0**
ΔI neat-DVB	−30.8	22.2	76.6	43.0	−32.3	**15.7**
ΔI 3-ZMOF@DVB	−35.1	7.1	27.7	14.9	−34.4	**−4.0**
ΔI 5-ZMOF@DVB	−44.3	−5.0	19.5	7.1	−42.7	**−13.1**
ΔI HP-5MS	31.0	68.0	62.0	95.0	63.0	**64.0**
ΔI SWNT	−63.0	100	125	—	176	**—**

Measured at 100 °C for neat-DVB and 180 °C for ZMOF@DVB monoliths. X', Y', Z', U', and S' represent benzene,1-butanol, 2-pentanone, 1-nitropropane, and pyridine, respectively. Average related to the total polarity of the material.

3.3. Improved chromatographic separation of small molecules

The chromatographic performance range of the monolithic composite was examined by the separation of aliphatic, aromatic, cyclic, acidic, and basic compounds, and light hydrocarbon gasses. A baseline separation of linear alkanes mixture (pentane, hexane, heptane, and octane) was obtained at 150 °C and 0.5 MPa column pressure, using 3-ZMOF@DVB and 5-ZMOF@DVB composite monoliths with increasing performance and higher retention as ZMOF content increased, reflecting an elevated hydrophobic nature of the composite material (Fig. 3A). In contrast, the neat DVB monolith could not completely separate the linear alkanes mixture under similar conditions. Decreasing retention time as column temperature increases for both the polymer monolith and the composite monolith indicates an exothermic separation process (Fig. S5). The linear relations in the Van't Hoff plots (R^2: 0.970 – 0.999) indicated that there was no change in the mechanism of interaction over the measured temperature range for the three monoliths (Fig. S6)

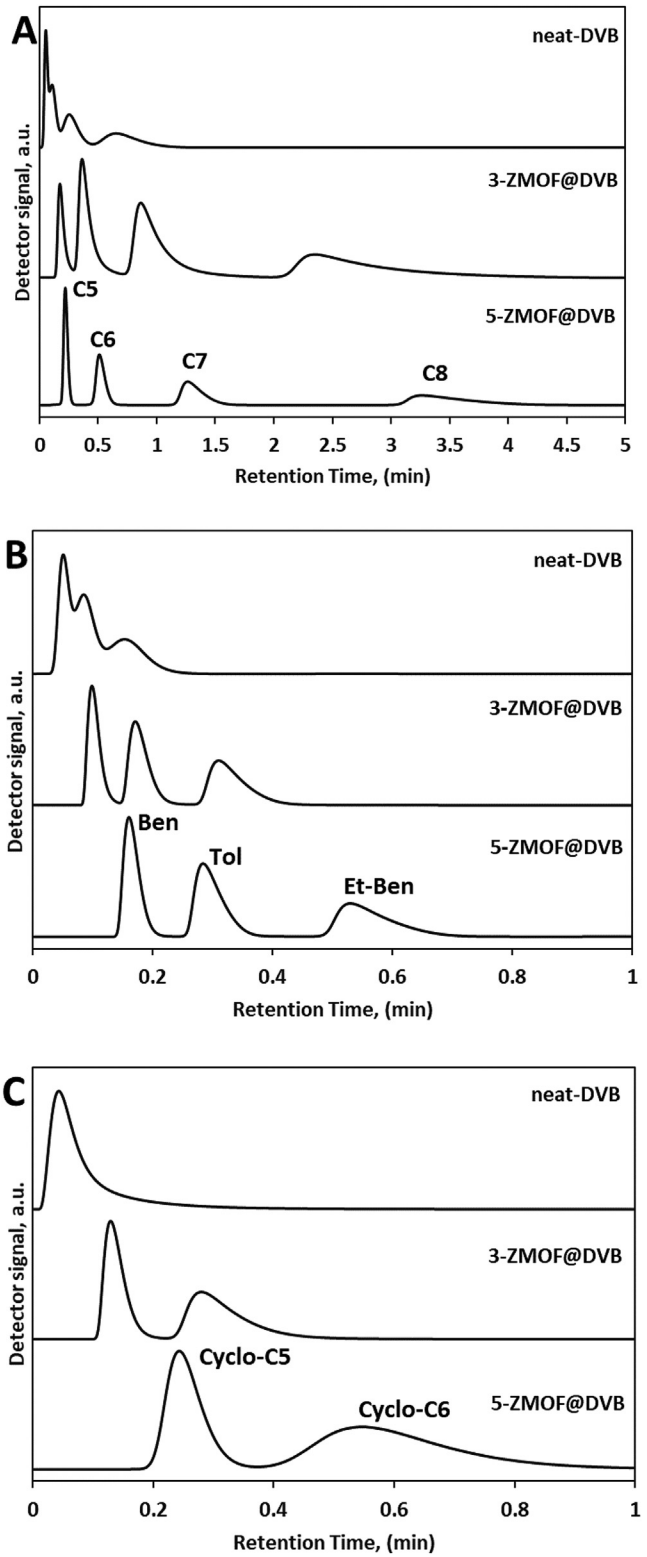

Fig. 3. Gas chromatograms of neat-DVB, 3-ZMOF@DVB, and 5-ZMOF@DVB monolithic columns (18 cm long × 0.25 mm inner diameter) separations under constant helium pressure of 0.5 MPa. (A) pentane (C5), hexane (C6), heptane (C7), and octane (C8) at 150 °C; (B) benzene (Ben), toluene (Tol), and ethyl benzene (Et-Ben) at 200 °C; (C) cyclopentane (Cyclo-C5) and cyclohexane (Cyclo-C5) at 150 °C. Injection volume 1μL headspace vapor.

Table 2
Resolution and separation factor of three pairs of linear alkane separation (Pentane/Hexane, Hexane/Heptane, and Heptane/Octane) using neat-DVB, 3-ZMOF@DVB, and 5-ZMOF@DVB monolithic columns (18 cm long × 0.25 mm inner diameter) at 120 °C and 0.5 MPa.

Resolution	Pentane/Hexane	Hexane/Heptane	Heptane/Octane
neat-DVB	0.79	0.97	1.10
3-ZMOF@DVB	1.35	1.77	1.98
5-ZMOF@DVB	2.94	3.39	3.53
Separation Factor			
neat-DVB	2.91	2.96	3.04
3-ZMOF@DVB	2.72	2.97	3.36
5-ZMOF@DVB	3.14	3.12	3.13

A dramatic increase in resolution was observed between linear alkane pairs when utilizing the composite monolithic materials for separation (Table 2). However, the degree of resolution enhancement decreased as the aliphatic chain length increased, indicating better separation performance improvement toward lighter hydrocarbons (3.7, 3.5, and 3.2 times resolution enhancement from neat-DVB to 5-ZMOF@DVB for pentane/hexane, hexane/heptane and heptane/octane, respectively).

Strong retention and higher resolution were associated with incorporating ZMOF nanoparticles into DVB monolithic matrix for a mixture of benzene, toluene, and ethylbenzene (Fig. 3B), revealing the effect of $\pi-\pi$ van der Waals interactions in the separation of aromatics. The neat-DVB control column could not separate a cyclopentane/cyclohexane mixture at 150 °C. In comparison, the composite monolithic stationary phases separated the cycloalkanes mixture at the same temperature (Fig. 3C). An excellent fast high-resolution separation for six members linear alkanes mixture (pentane, hexane, heptane, octane, nonane, and decane) was obtained within 1.8 min using a temperature program on 5-ZMOF@DVB (Fig. 4A). As a proof of concept, a mixture of light alkane gasses was completely separated (Fig. 4B) using the same temperature program and the same column. ZMOF nanoparticles brought a new dimension of separation to the monolithic matrix through their sub-nano size pore opening.

Fig. 4C shows a perfect separation for a mixture of polar probes under isothermal conditions of 100 °C. However, the elution order of polar probes didn't obey the expected elution order according to boiling points; instead, the polarity of separated analytes significantly affected their retention behavior in agreement with the McReynolds constants study (Table S1). For example, the highest polarity probe, acetonitrile, was the first to elute from the 5-ZMOF@DVB column, followed by other polar probes as polarity decreases except for two exceptions; diethyl ether and pyridine. The low boiling point of diethyl ether (34.5 °C) affected its elution order which is supposed to be the last analyte to elute, as it is the lower polarity probe (dipole moment = 13). On the contrary, the relatively high boiling point has forced pyridine to become the latest eluted probe despite its higher dipole moment than diethyl ether, tetrahydrofuran, and ethyl acetate (Table S1). It is worth noting that the elution order of a similar mixture of polar compounds using the neat-DVB column had the same elution order with eight times lower total retention time but with 2.3−5.1 lower resolution and almost no separation of diethyl ether and tetrahydrofuran (Table S1). Asymmetric peaks were noticed for some of the tested probes, which may be attributed to the present of silanol residues within the dead volume of the fused silica tubing and relatively low pressure. Furthermore, the large particle size and pore volume could contribute to poor interactions and hence a higher degree of peak tailing. Therefore, increasing the percentage of ZMOF in 5-ZMOF@DVB led to lower peak tailing as a result of increased surface area by reducing microglobules and pore volume (Fig. 3). The

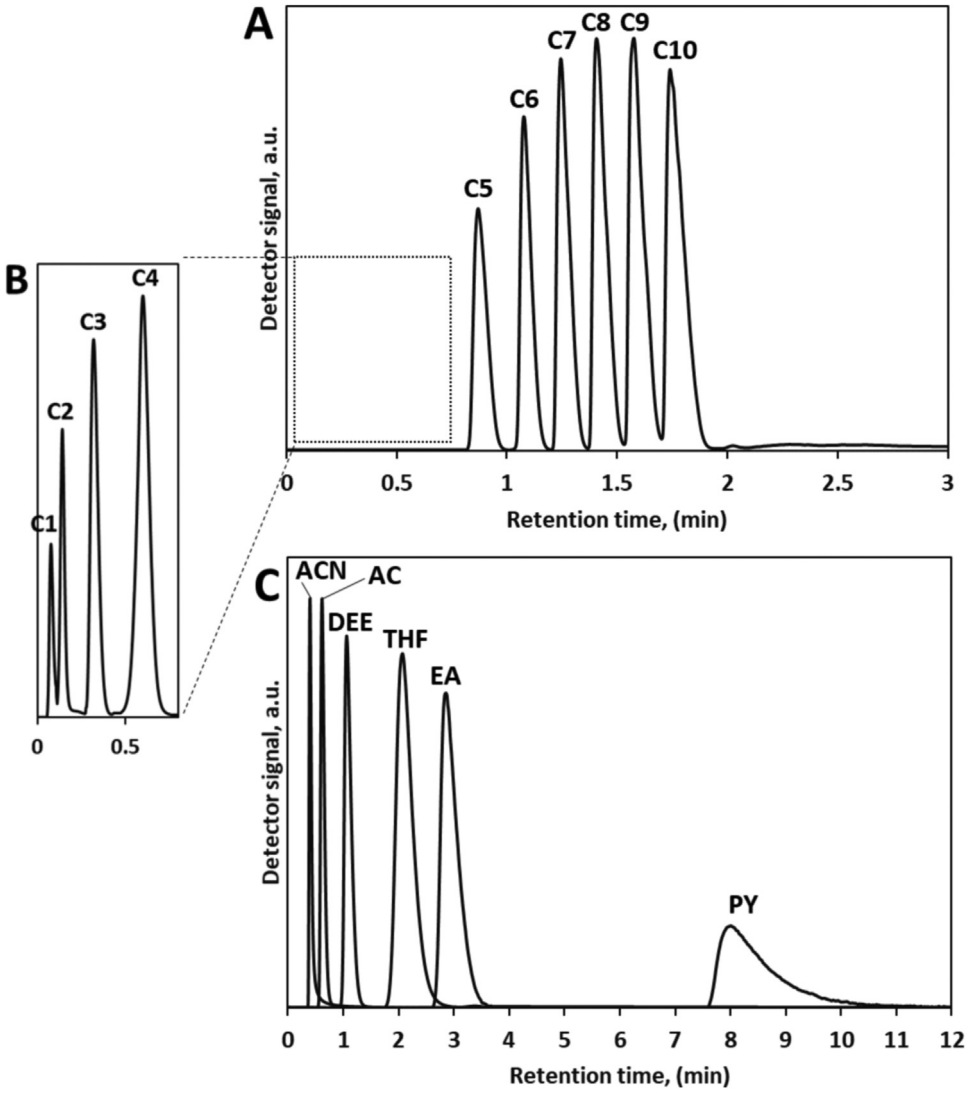

Fig. 4. Gas chromatograms of 5-ZMOF@DVB monolithic column (18 cm long × 0.25 mm inner diameter) separations under constant helium pressure of 0.5 MPa. (A) pentane (C5), hexane (C6), heptane (C7), octane (C8), nonane (C9), and decane (C10); (B) methane (C1), ethane (C2), propane (C3) and butane (C4); temperature program for both A and B: started with 40 °C, followed by heating to 120 °C at 100 °C min^{-1}, then heating to 300 °C at 200 °C min^{-1}; (C) acetonitrile (ACN), acetone (AC), diethylether (DEE), tetrahydrofuran (THF), ethyl acetate (EA), and pyridine (PY) at100 °C isothermal conditions. Injection volume 1μL headspace vapor.

tailing of the produced peaks could also be reduced using a temperature program instead of isothermal conditions (Fig. S7).

3.4. Column efficiency

Van Deemter curve comparison between the neat-DVB monolith and the composite monoliths showed a remarkable improvement in column efficiency in terms of the height equivalent of theoretical plates (HETP) (Fig. 5). The HETP for hexane separation using 5-ZMOF@DVB composite column was calculated and plotted against the change in flow rate in the range 0.032–2.78 mL min^{-1}. The flow rates were measured using a bubble flowmeter over a constant pressure ranging from 0.02 to 0.6 MPa and isothermal conditions under 200 °C. As a result, an optimum plate height of 1.75 mm (571 plates m^{-1}) and 1.21 mm (823 plates m^{-1}) was determined for 3-ZMOF@DVB and 5-ZMOF@DVB, respectively. In comparison, a significantly higher HETP of 5.82 mm (189 plates m^{-1}) was measured for the neat-DVB column. Generally, the column efficiency increased with increasing ZMOF percentage within the monolithic composite at similar conditions.

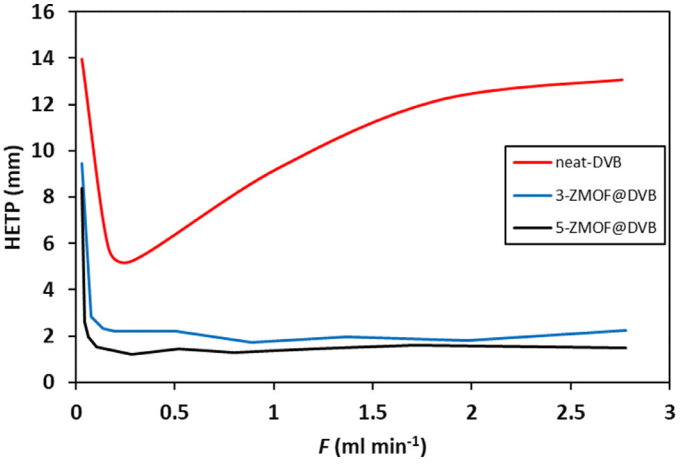

Fig. 5. The Van Deemter plots relating the height equivalent of theoretical plates (HETP) and the carrier gas (helium) flow rate for neat-DVB, 3-ZMOF@DVB, and 5-ZMOF@DVB monolithic columns (18 cm long × 0.25 mm inner diameter) for hexane over a pressure ranging from 0.02 to 0.6 MPa and isothermal conditions under 200 °C.

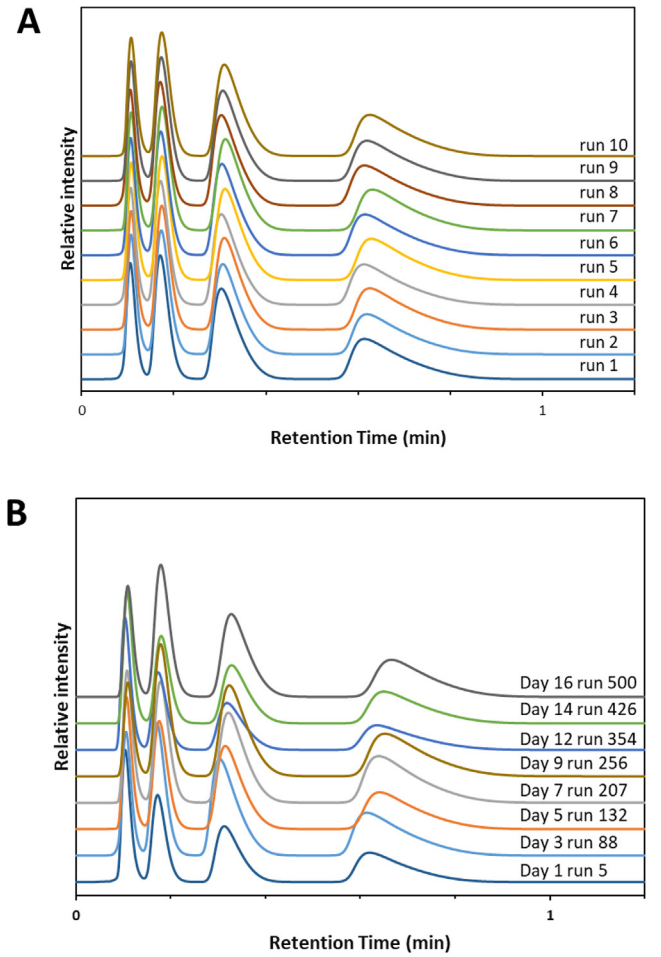

Fig. 6. (A) Repeatability (run-to-run) over 10 runs, and (B) Reproducibility (day-to-day) over 16 days and 500 runs, for a mixture of linear alkanes (pentane, hexane, heptane, and octane) using 5-ZMOF@DVB column (18 cm long × 0.25 mm inner diameter) under 190 °C and 0.5 MPa.

One of the most advantageous characteristics of a monolithic column over packed or open tubular columns is its low interface mass transfer with an increasing flow rate leading to a flat Van Deemter curve and stable HETP even with increasing flow rate [46]. Exceptionally, the neat-DVB didn't perform as a typical monolithic column and showed a declining efficiency after the optimum flow rate (Fig. 5). This is mainly because the preparation conditions for the neat-DVB column were chosen carefully to form a highly permeable monolith with a predominant macroporous structure. Additionally, the absence of a monofunctional monomer within the prepared monolithic structure was found to significantly affect the steepness of the right branch of the Van Deemter curve; as the monofunctional monomer percentage increases, the Van Deemter curve becomes steeper [20]. However, incorporating sod-ZMOF nanoparticles into the monolithic network restored its Van Deemter reduced C term, allowing faster separations with the same high efficiency (Fig. 5).

3.5. Column repeatability and reproducibility

Excellent repeatability was determined for the 5-ZMOF@DVB column for four-membered alkane series separation (pentane to octane) under 190 °C and 0.5 MPa (Fig. 6A). The relative standard deviation (RSD%) calculations of pentane and octane for ten replicates were 0.65% and 1.03% for retention time, 1.08% and 1.10% for retention factor, and 5.18% and 4.64% for peak width at half height, respectively (Table S2). The column retains its efficiency over ten replicates with 11.39% and 8.25% HETP RSD% for pentane and octane, respectively. 5-ZMOF@DVB also shows good reproducibility through ten days and over more than 500 runs with RSD% of pentane and octane in the range 2.25–3.3, 3.53–3.75, 5.27–5.36 and 9.19–11.39 for retention time, retention factor, width at half height and HETP, respectively (Fig. 6B). In addition, inter-batch reproducibility exhibited excellent reproducibility for three 5-ZMOF@DVB similar columns, as demonstrated in Table S2, confirming a repeatable synthetic strategy and usability as analytical chromatography stationary phase. The outstanding repeatability and reproducibility of ZMOF@DVB monolithic material could be attributed to its high thermal stability, as verified by the TGA study, and to the stable crystalline structure of sod-ZMOF, as demonstrated with PXRD measurements.

Propane gas was utilized as a test probe under 100 °C isothermal conditions and 0.5 MPa to examine loading capacity of the developed stationary phases under routine use and its applicability to quantitative analysis. A linear consistency was noticed in retention, initial and final time of propane peak, as well as its 1st moment, with increasing injection volume up to 100 μL (Fig. 7A). Furthermore, a linear dependence of peak area with injection volume was confirmed up to 20 μL with a linear correlation coefficient of 0.996 (Fig. 7B) (Table S3).

3.6. Qualitative analysis of commercial butane sample

Three commercial Lighter gas cartridges were analyzed, one from a local producer and two imported cartridges, to identify their gas content via comparison with the retention time of pure gasses injected under the same conditions. Gas cartridges usually contain a mixture of 70–80% butane and 20–30% propane. The addition of propane aims to increase the pressure of the cartridge to keep the mixture in a gaseous state, especially in sub-zero cold weather, which is not the usual local climate. Fig. 8 reveals five components in the gas mixture from the first cartridge provided by a local manufacturer (local sample). Complete separation of the local sample was performed using the 5-ZMOF@DVB composite monolithic column under an isothermal condition of 60 °C and a constant pressure of 0.3 MPa with a resolution ranging from 0.83 to 3.13 (Table S4). Surprisingly, the gas mixture content of butane was found to consist of both isobutane and butane with a relative peak area percentage of 28.75% and 38.31%, respectively, corresponding to a total percentage of 66.96%, which is close enough to the butane content prescribed in the mixture. The examined column could differentiate between butane and isobutene with an acceptable resolution (0.83) and a selectivity of 1.48. Butane/isobutane selectivity was probably due to the molecular sieving effect recently revealed using a ZMOF-based membrane [31]. A percentage of 32.45% of propane was determined in the local sample, which is also close to the prescribed content of propane. Additionally, trace amounts of methane and ethane were detected (Table S4).

The other two samples were from imported gas cartridges, and the same isobutane/butane mixture was detected, such as the local sample instead of only butane as prescribed (Fig. S8A, B). The total butane content in imported sample 1 was 97.44% as an isobutane/butane mixture plus 2.39% propane, while it supposes to contain only butane. The third sample (imported sample 2) included 98.06% total butane, as an isobutane/butane mixture, and 1.89% propane, while the note on the can mentioned content of 20/80% propane/butane. Although it probably may not affect the performance of the Lighter gas mixture, imported sample 2 imprecisely mentioned a way higher propane content than it actually has, and all three samples did not note that butane content is a mixture of isobutene and butane. The local gas cartridge provider sticks with

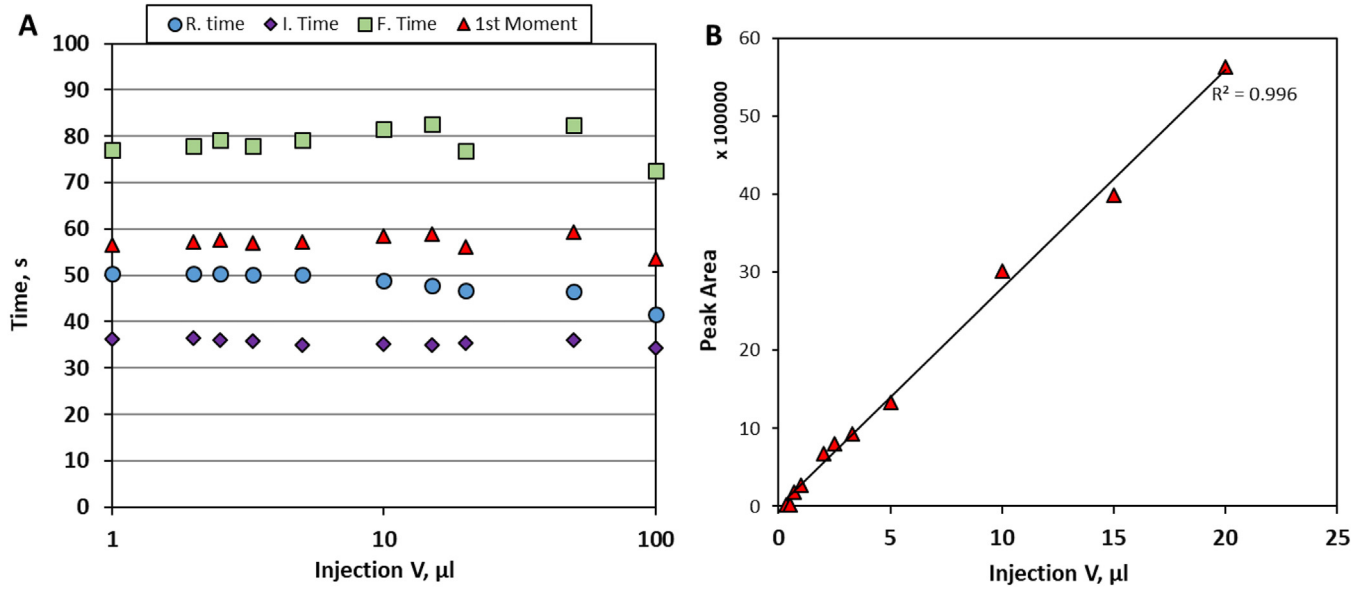

Fig. 7. Column loading study for 5-ZMOF@DVB column (18 cm long × 0.25 mm inner diameter) using propane as a testing probe under 100 °C and 0.5 MPa. (A) linear consistency of retention, initial and final time of propane peak, as well as its 1st moment, with increasing injection volume in a log scale, and (B) linear consistency of propane peak area with increasing injection volume.

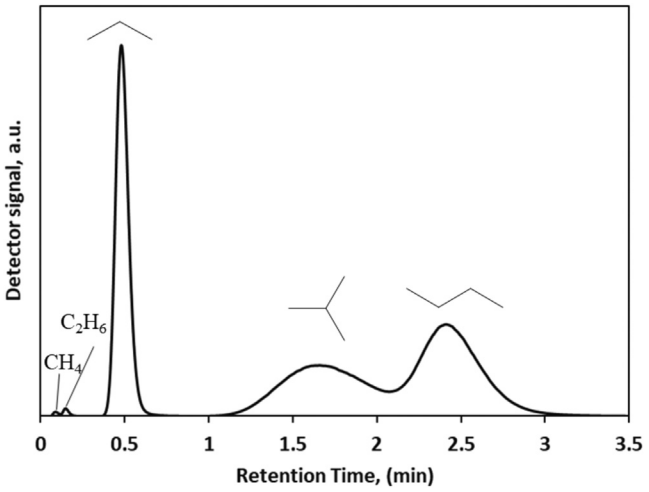

Fig. 8. Separation of a commercial Lighter Gas sample using 5-ZMOF@DVB column (18 cm long × 0.25 mm inner diameter) under an isothermal temperature of 60 °C and inlet pressure 0.3 MPa. Peaks: methane, ethane, propane, isobutane, and butane, respectively, according to elution order.

the internationally recommended percentage of propane/butane mixture (30/70%), which they clearly wrote on the cartridges; however, using the other two imported Lighter gas mixtures would be safer in such a hot climate like in Saudi Arabia.

3.7. R-410A azeotropic mixture separation

The previous performance of the ZMOF@DVB composite stationary phase has encouraged the exploration of more challenging separations, such as the azeotropic refrigerant mixture of difluoromethane (R-32) and pentafluoroethane (R-125) (50/50 wt%), commercially known as Freon R-410A. The importance of such separation arises from the greenhouse effect of fluorocarbons due to their high global warming potential (GWP) and hence the persistent need for energy-efficient separation, reclamation, and recovery technologies through adsorption-based separation [47]. The main reason behind the frustrating difficulty in separating the R-410A mixture is the boiling point similarity of its components (Table S5). Nevertheless, complete separation of the R-32 and R-125 blends was achieved with a selectivity of 3.36 and a resolution of 1.1 (Table S6), using the 3-ZMOF@DVB column under room temperature (32 °C) and constant helium pressure of 0.5 MPa (Fig. 9A). In addition, the 5-ZMOF@DVB column was also able to separate the mixture under the same conditions with higher selectivity (3.48) but with lower resolution (0.57) due to broadening of R-125 peak (Table S6). R-125 peaks broadened about 2.3 to 3.4 times using the 5-ZMOF@DVB column compared to the 3-ZMOF@DVB column, while the R-32 peak kept the same broadening indicating more distribution of R-125 molecules as ZMOF Percentage increased. The simulated adsorption isotherm for sod-ZMOF confirmed that the separation ability is attributed to the incorporated nanoparticles (Fig. 9B), considering the neat-DVB monolith's failure to afford any separation. The simulated uptake showed preferential adsorption of R-125 over R-32 in agreement with their chromatographic elution order. Furthermore, the adsorption isotherm shape gave evidence of a thermodynamically driven separation rather than a molecular sieving separation, such as the previous case with butane isomers.

Thermodynamic parameters were evaluated for the adsorptive separation of R-32 and R-125 at infinite dilution (Henry's region) and a temperature range of 32–60 °C for a deeper understanding of the separation mechanism. Initially, it was observed that the adjusted retention time of analytes reduced significantly when the column temperature increased, implying exothermic adsorption. Van't Hoff plots exhibited a high linear correlation (Fig. 10), indicating that the interaction mechanism did not alter during the separation process. Negative Gibbs free energy (ΔG_A) values (Table 3 and S10) indicate a spontaneous process of solutes transfer from the mobile phase to the stationary phase for both monoliths.

The slope of plots of $\ln V_g$ vs. $1/T$ was used to calculate adsorption enthalpies (ΔH_A) (Fig. S9), with a linear dependency indicating a constant value of ΔH_A in the temperature range investigated (32–60 °C). ΔH_A values over both studied composites are higher than the enthalpy change of liquefaction (ΔH_{liq}) [48] (Table 3 and S11), confirming that interactions between adsorbates and adsorbent are overwhelming the adsorbate–adsorbate interactions. Furthermore, as these values are so close, it was also

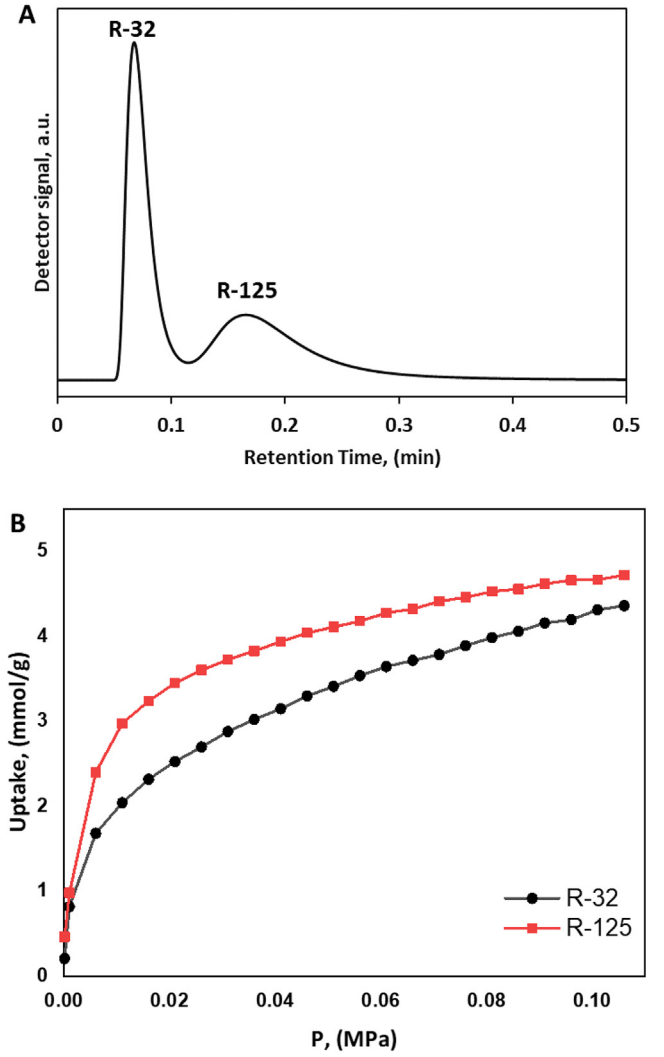

Fig. 9. (A) Chromatograms of difluoromethane (R-32) and pentafluoroethane (R-125) separation using 3-ZMOF@DVB column (18 cm long × 0.25 mm inner diameter) under 32 °C and constant helium pressure of 0.5 MPa, (B) simulated R-32 and R-125 adsorption isotherms for sod-ZMOF.

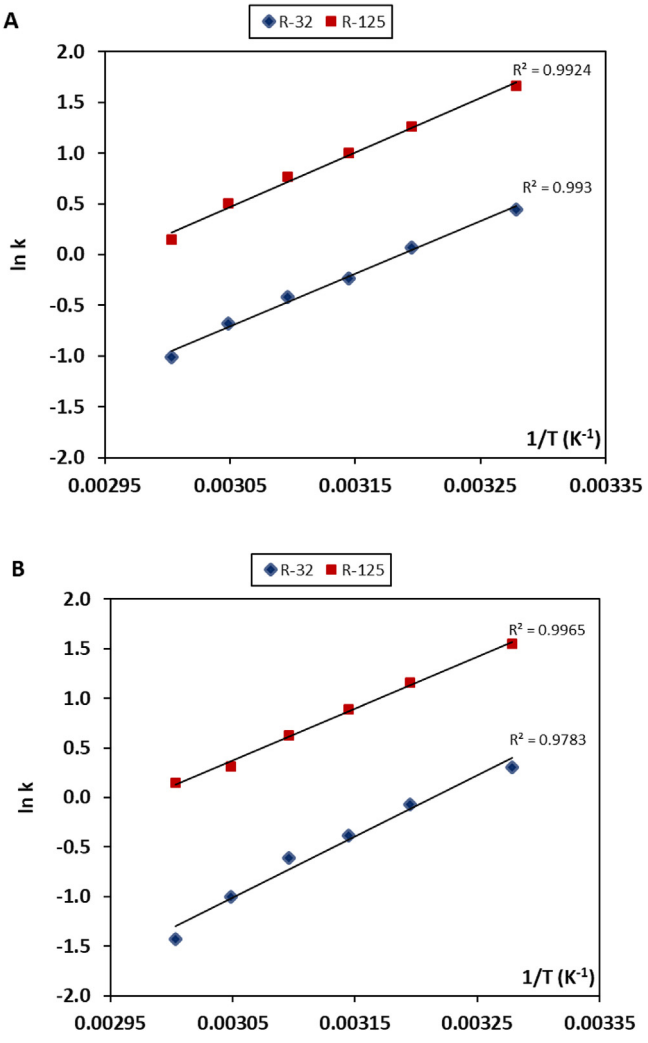

Fig. 10. Van't Hoff plots of difluoromethane (R-32) and pentafluoroethane (R-125), on (A) 3-ZMOF@DVB, and (B) 5-ZMOF@DVB columns, in the range 32–60 °C. Data was recorded at 0.5 MPa.

Table 3
Free energy change of adsorption (ΔG_A) and entropy change of adsorption (ΔS_A) at 50 °C, and the enthalpy change of adsorption (ΔH_A) at the range 32–60 °C, of difluoromethane (R-32) and pentafluoroethane (R-125), on 3-ZMOF@DVB, and 5-ZMOF@DVB columns. Data was recorded at 0.5 MPa.

	$-\Delta G_A$ (kJ mol^{-1})		$-\Delta S_A$ (J mol^{-1} K^{-1})		$-\Delta H_A$ (kJ mol^{-1})	
Columns	R-32	R-125	R-32	R-125	R-32	R-125
3-ZMOF@DVB	19.87	23.91	72.5	65.1	43.30	43.94
5-ZMOF@DVB	17.61	21.81	115.1	77.8	54.79	46.94

proved that weak secondary van der Waals forces drive most interactions across the surface. As a result, it is feasible to conclude that the surface of both ZMOF@DVB monoliths is energetically homogenous toward the adsorption of the designated analytes. The enthalpy change of adsorption is commonly used to discriminate between physical and chemical adsorption, with an arbitrary value of 62.8 kJ mol^{-1} [49]. However, Table 3 demonstrates that the values of ΔH_A do not surpass the physical-chemical adsorption limit, showing that all testing probes solely interact physically with the studied stationary phases.

The absolute value of the enthalpy of adsorption for R-32 and R-125 was almost the same for the adsorptive separation over 3-ZMOF@DVB and even higher for R-32 than R-125 using 5-ZMOF@DVB. The higher dipole moment of R-32 was probably the reason for the higher ΔH_A values with an increasing percentage of the anionic sod-ZMOF within the composite structure. Accordingly, R-32 was supposed to retain more than R-125, which is not the actual situation. Given that the pore diameter of sod-ZMOF is 4.1 Å and the kinetic diameter of R-125 is 4.4 Å, a higher retention of R-125 in sod-ZMOF was anticipated. R-125 molecules were probably trapped due to steric hindrance occurring during the sod-ZMOF desorption process. This would be explained by the lower values of entropy of adsorption of R-125 than R-32 (Table 3 and S12), indicating a higher degree of freedom for R-125 inside the pore cavity of sod-ZMOF allowing for more adsorbate-adsorbent (C–F···M/ C–H···π) interactions. Taken together, the separation of R-410A azeotropic mixture over ZMOF@DVB composite monolith with preferential adsorption of R-125 was mainly due to its trapping inside ZMOF pores with an entropic advantage represented in more freedom and resulting in increasing distribution with stronger adsorption and higher retention. Comparison between 3-ZMOF@DVB and 5-ZMOF@DVB exhibited higher values of the enthalpy and entropy of adsorption for the latter for both R-32 and R-125, confirming the pivotal role effect of sod-ZMOF nanoparticles in separation.

4. Conclusions

We prepared sod-ZMOF@DVB monolithic composite capillary columns (18 cm long × 0.25 mm inner diameter) for conventional GC applications of aliphatic, aromatic, cyclic, acidic, basic compounds, and light hydrocarbon, and fluorocarbon gasses separations under relatively low-pressure (0.5 MPa). The prepared columns showed satisfying thermal stability up to 380 °C, and the BET surface area of the DVB polymer monolith almost doubled by adding only 1.17 wt% of sod-ZMOF nanoparticles (225 nm) into the monolithic matrix. A fast high-resolution separation of linear alkanes sample was performed within 2 min for a line alkanes mixture from methane to decane. McReynolds constants study revealed an increasing nonpolar nature of the prepared composite with increasing sod-ZMOF percentage, which is a desirable character for most chromatographic applications. A mixture of polar probes was separated successfully with an elution order that obeys its content decreasing polarity consistent with McReynolds constants results. Excellent repeatability and reproducibility were demonstrated over more than 500 runs and three batches of columns. Commercial samples of a Lighter gas mixture were qualitatively analyzed to identify its gas content and percentage. The composite monolithic column 5-ZMOF@DVB completely separated the Lighter gas mixture content, including butane and isobutene. Finally, the ZMOF@DVB composite showed a preferential selectivity of R-125 over R-32, probably due to the entropic advantage of R-125, allowing for more freedom and hence more interaction while trapped inside the ZMOFs pore cavity.

Taken together, these results demonstrate the advantage of combining the high permeability and simple preparation of monoliths with high surface area, designable structure, and wide variability of MOFs. ZMOF@DVB composite allows for a higher resolution and performance separations of small molecules by increasing the surface area of interaction and provides the monolithic matrix with well-defined nano-pores allowing for efficient gas separations. Additionally, the sod-ZMOFs anionic structure can be utilized for *in-situ* post-synthetic modifications through cation exchange to extend the application of the monolithic composite toward specific separations. On the other hand, GC provided an effective tool for the initial evaluation of porous polymers' adsorption and separation efficiency and as an alternative practical approach rather than calculation methods such as IAST. This work paves the way for intriguing research series to explore the separation efficiency of more ZMOF topologies, molecular sieving possibilities, and *in-situ* post-synthetic modifications of the composite monolith.

Declaration of Competing Interest

The authors declare that they have no known competing financial interests or personal relationships that could have appeared to influence the work reported in this paper.

CRediT authorship contribution statement

Kareem Yusuf: Conceptualization, Methodology, Software, Data curation, Writing – original draft, Writing – review & editing. **Osama Shekhah:** Conceptualization, Writing – original draft, Investigation. **Ahmad Aqel:** Software, Validation. **Seetah Alharbi:** Methodology. **Ali S. Alghamdi:** Methodology. **Reem M. Aljohani:** Visualization, Methodology. **Mohamed Eddaoudi:** Supervision. **Zeid A. ALOthman:** Supervision.

Data availability

Data will be made available on request.

Acknowledgments

This work was supported through the project funded by the National Plan of Science, Technology and Innovation (MAARIFAH), King Abdulaziz City for Science and Technology, Kingdom of Saudi Arabia, Grant Number 14-ADV2447–02.

Supplementary materials

Supplementary material associated with this article can be found, in the online version, at doi:10.1016/j.chroma.2023.463922.

References

[1] H.C. Zhou, J.R. Long, O.M. Yaghi, Introduction to metal-organic frameworks, Chem. Rev. 112 (2012) 673–674, doi:10.1021/CR300014X/ASSET/IMAGES/MEDIUM/CR-2012-00014X_0003.GIF.
[2] X. Zhang, Z. Chen, X. Liu, S.L. Hanna, X. Wang, R. Taheri-Ledari, A. Maleki, P. Li, O.K. Farha, A historical overview of the activation and porosity of metal–organic frameworks, Chem. Soc. Rev. 49 (2020) 7406–7427, doi:10.1039/D0CS00997K.
[3] H. Furukawa, K.E. Cordova, M. O'Keeffe, O.M. Yaghi, The chemistry and applications of metal-organic frameworks, Science (80) (2013) 341 -., doi:10.1126/SCIENCE.1230444/SUPPL_FILE/FURUKAWA.SM.CORRECTED.PDF.
[4] M. Safaei, M.M. Foroughi, N. Ebrahimpoor, S. Jahani, A. Omidi, M. Khatami, A review on metal-organic frameworks: synthesis and applications, TrAC Trends Anal. Chem. 118 (2019) 401–425, doi:10.1016/J.TRAC.2019.06.007.
[5] X. Li, X. Yang, H. Xue, H. Pang, Q. Xu, Metal–organic frameworks as a platform for clean energy applications, EnergyChem. 2 (2020) 100027, doi:10.1016/J.ENCHEM.2020.100027.
[6] S. Rojas, P. Horcajada, Metal-organic frameworks for the removal of emerging organic contaminants in water, Chem. Rev. 120 (2020) 8378–8415, doi:10.1021/ACS.CHEMREV.9B00797/ASSET/IMAGES/LARGE/CR9B00797_0009.JPEG.
[7] K. Yusuf, A. Aqel, Z. ALOthman, Metal-organic frameworks in chromatography, J. Chromatogr. A 1348 (2014) 1–16, doi:10.1016/J.CHROMA.2014.04.095.
[8] F. Svec, A.A. Kurganov, Less common applications of monoliths: III. Gas chromatography, J. Chromatogr. A 1184 (2008) 281–295, doi:10.1016/J.CHROMA.2007.07.014.
[9] W.Q. Tang, J.Y. Xu, Z.Y. Gu, Metal–organic-framework-based gas chromatographic separation, Chem. An Asian J. 14 (2019) 3462–3473, doi:10.1002/ASIA.201900738.
[10] Z. Zajickova, I. Špánik, Applications of monolithic columns in gas chromatography and supercritical fluid chromatography, J. Sep. Sci. 42 (2019) 999–1011, doi:10.1002/JSSC.201801071.
[11] F. Svec, K.K. Králov, K. Králové, C. Republic, Monolithic columns: a historical overview, Electrophoresis 38 (2017) 2810–2820, doi:10.1002/ELPS.201700181.
[12] F. Svec, Y. Lv, Advances and recent trends in the field of monolithic columns for chromatography, Anal. Chem. 87 (2015) 250–273, doi:10.1021/AC504059C/ASSET/IMAGES/LARGE/AC-2014-04059C_0009.JPEG.
[13] M.R. Gama, F.R.P. Rocha, C.B.G. Bottoli, Monoliths: synthetic routes, functionalization and innovative analytical applications, TrAC Trends Anal. Chem. 115 (2019) 39–51, doi:10.1016/J.TRAC.2019.03.020.
[14] S. Eeltink, D. Meston, F. Svec, Recent developments and applications of polymer monolithic stationary phases, Anal. Sci. Adv. 2 (2021) 250–260, doi:10.1002/ANSA.202100006.
[15] A. Kurganov, Monolithic column in gas chromatography, Anal. Chim. Acta 775 (2013) 25–40, doi:10.1016/J.ACA.2013.02.039.
[16] F. Svec, Organic polymer monoliths as stationary phases for capillary HPLC, J. Sep. Sci. 27 (2004) 1419–1430, doi:10.1002/JSSC.200401825.
[17] Y. Peng, W. Yang, Y. Peng, W.S. Yang, 2D metal-organic framework materials for membrane-based separation, Adv. Mater. Interfaces 7 (2020) 1901514, doi:10.1002/ADMI.201901514.
[18] K. Yusuf, A. Aqel, Z. Alothman, A.Y. Badjah-Hadj-Ahmed, Preparation and characterization of alkyl methacrylate-based monolithic columns for capillary gas chromatography applications, J. Chromatogr. A 1301 (2013) 200–208, doi:10.1016/j.chroma.2013.05.060.
[19] K. Yusuf, A.Y. Badjah-Hadj-Ahmed, A. Aqel, Z.A. ALOthman, Fabrication of zeolitic imidazolate framework-8-methacrylate monolith composite capillary columns for fast gas chromatographic separation of small molecules, J. Chromatogr. A 1406 (2015) 299–306, doi:10.1016/J.CHROMA.2015.06.026.
[20] K. Yusuf, A.Y. Badjah-Hadj-Ahmed, A. Aqel, T. Aouak, Z.A. Alothman, Zeolitic imidazolate framework-methacrylate composite monolith characterization by inverse gas chromatography, J. Chromatogr. A 1443 (2016) 233–240, doi:10.1016/J.CHROMA.2016.03.025.
[21] A. Aqel, A.A. Ghfar, K. Yusuf, K.M. Alotaibi, R.M. Alafra'a, M.A. Habila, A.Y. Badjah-Hadj-Ahmed, Z.A. Alothman, Montmorillonite-based polymethacrylate composite monoliths as stationary phase materials for food and pharmaceutical analysis in capillary liquid and gas chromatography, J. Chromatogr. A (2022) 463695, doi:10.1016/J.CHROMA.2022.463695.
[22] A. Aqel, M. Obbed, A.A. Ghfar, K. Yusuf, A.M. Alsubhi, A. Badjah-Hadj-Ahmed, Naturally occurring montmorillonite-based polymer monolith composites as stationary phases for capillary liquid and gas chromatography, Separations 9 (2022) 389, doi:10.3390/SEPARATIONS9120389.

[23] M. Eddaoudi, D.F. Sava, J.F. Eubank, K. Adil, V. Guillerm, Zeolite-like metal–organic frameworks (ZMOFs): design, synthesis, and properties, Chem. Soc. Rev. 44 (2014) 228–249, doi:10.1039/C4CS00230J.
[24] K. Egeblad, C.H. Christensen, M. Kustova, C.H. Christensen, Templating mesoporous zeolites, Chem. Mater. 20 (2008) 946–960, doi:10.1021/CM702224P/ASSET/IMAGES/LARGE/CM-2007-02224P_0008.JPEG.
[25] D. Chen, Y. Zhou, J. Zhong, A review on Mn^{4+} activators in solids for warm white light-emitting diodes, RSC Adv. 6 (2016) 86285–86296, doi:10.1039/C6RA19584A.
[26] P.B. Venuto, Organic catalysis over zeolites: a perspective on reaction paths within micropores, Microporous Mater. 2 (1994) 297–411, doi:10.1016/0927-6513(94)00002-6.
[27] B.A. Al-Maythalony, O. Shekhah, R. Swaidan, Y. Belmabkhout, I. Pinnau, M. Eddaoudi, Quest for anionic MOF membranes: continuous sod -ZMOF membrane with CO_2 adsorption-driven selectivity, J. Am. Chem. Soc. 137 (2015) 1754–1757, doi:10.1021/JA511495J/SUPPL_FILE/JA511495J_SI_001.PDF.
[28] A. Kiliç, Ç. Atalay-Oral, A. Sirkecioğlu, S.B. Tantekin-Ersolmaz, M.G. Ahunbay, Sod-ZMOF/Matrimid® mixed matrix membranes for CO_2 separation, J. Memb. Sci. 489 (2015) 81–89, doi:10.1016/J.MEMSCI.2015.04.003.
[29] G. Liu, Y. Labreche, V. Chernikova, O. Shekhah, C. Zhang, Y. Belmabkhout, M. Eddaoudi, W.J. Koros, Zeolite-like MOF nanocrystals incorporated 6FDA-polyimide mixed-matrix membranes for CO_2/CH4 separation, J. Memb. Sci. 565 (2018) 186–193, doi:10.1016/J.MEMSCI.2018.08.031.
[30] B. Demir, M.G. Ahunbay, Propane/propylene separation in ion-exchanged zeolite-like metal organic frameworks, Microporous Mesoporous Mater. 198 (2014) 185–193, doi:10.1016/J.MICROMESO.2014.07.028.
[31] V. Chernikova, O. Shekhah, Y. Belmabkhout, M. Karunakaran, M. Eddaoudi, A zeolite-like metal-organic framework based membrane for reverse selective hydrogen separation and butane isomers sieving, Angew. Chem. Int. Ed. (2023) e202218842, doi:10.1002/ANIE.202218842.
[32] D. Peralta, G. Chaplais, A. Simon-Masseron, K. Barthelet, C. Chizallet, A.A. Quoineaud, G.D. Pirngruber, Comparison of the behavior of metal-organic frameworks and zeolites for hydrocarbon separations, J. Am. Chem. Soc. 134 (2012) 8115–8126, doi:10.1021/JA211864W/SUPPL_FILE/JA211864W_SI_001.PDF.
[33] M.I.H. Mohideen, Y. Belmabkhout, P.M. Bhatt, A. Shkurenko, Z. Chen, K. Adil, M. Eddaoudi, Upgrading gasoline to high octane numbers using a zeolite-like metal–organic framework molecular sieve with Ana-topology, Chem. Commun. 54 (2018) 9414–9417, doi:10.1039/C8CC04824J.
[34] K. Yusuf, O. Shekhah, Z. ALOthman, M. Eddaoudi, Metal-organic frameworks characterization via inverse pulse gas chromatography, Appl. Sci. 2021 11 (2021) 10243 Vol. 11, Page 10243, doi:10.3390/APP112110243.
[35] D. Peroni, R.J. Vonk, W. van Egmond, H.G. Janssen, Macroporous polymer monoliths as second dimension columns in comprehensive two-dimensional gas chromatography: a feasibility study, J. Chromatogr. A. 1268 (2012) 139–149, doi:10.1016/J.CHROMA.2012.10.019.
[36] M. Zabka, M. Minceva, A.E. Rodrigues, Experimental characterization and modelling of analytical monolithic column, J. Biochem. Biophys. Methods. 70 (2007) 95–105, doi:10.1016/J.JBBM.2006.10.002.
[37] L. Lavielle, J. Schultz, Surface properties of carbon fibers determined by inverse gas chromatography: role of pretreatment, Langmuir 7 (1991) 978–981, doi:10.1021/la00053a027.
[38] A.T. James, A.J. Martin, Gas-liquid partition chromatography; the separation and micro-estimation of volatile fatty acids from formic acid to dodecanoic acid, Biochem. J. 50 (1952) 679–690, doi:10.1042/bj0500679.
[39] J. Novák, Physicochemical measurement by gas chromatography, J. Chromatogr. A 187 (1980) 283–284, doi:10.1016/s0021-9673(00)87904-2.
[40] N.A. Katsanos, R. Thede, F. Roubani-Kalantzopoulou, Diffusion, adsorption and catalytic studies by gas chromatography, J. Chromatogr. A 795 (1998) 133–184, doi:10.1016/S0021-9673(97)00968-0.
[41] W.O. McReynolds, Characterization of some liquid phases, J. Chromatogr. Sci. 8 (1970) 685–691, doi:10.1093/CHROMSCI/8.12.685.
[42] A. Berthod, E.Y. Zhou, K. Le, D.W. Armstrong, Determination and use of Rohrschneider-McReynolds constants for chiral stationary phases used in capillary gas chromatography, Anal. Chem. 67 (2002) 849–857, doi:10.1021/AC00101A010.
[43] A.V. Kozin, A.A. Korolev, V.E. Shiryaeva, T.P. Popova, A.A. Kurganov, The influence of the natures of the carrier gas and the stationary phase on the separating properties of monolithic capillary columns in gas adsorption chromatography, Russ. J. Phys. Chem. A Focus Chem. 822 (82) (2008) 276–281, doi:10.1134/S0036024408020258.
[44] C. Lu, S. Liu, J. Xu, Y. Ding, G. Ouyang, Exploitation of a microporous organic polymer as a stationary phase for capillary gas chromatography, Anal. Chim. Acta 902 (2016) 205–211, doi:10.1016/j.aca.2015.10.034.
[45] M. Karwa, S. Mitra, Gas chromatography on self-assembled, single-walled carbon nanotubes, Anal. Chem. 78 (2006) 2064–2070, doi:10.1021/AC052115X.
[46] R. Hahn, M. Panzer, E. Hansen, J. Mollerup, A. Jungbauer, Mass transfer properties of monoliths, Sep. Sci. Technol. 37 (2007) 1545–1565, doi:10.1081/SS-120002736.
[47] A.D. Yancey, S.J. Terian, B.J. Shaw, T.M. Bish, D.R. Corbin, M.B. Shiflett, A review of fluorocarbon sorption on porous materials, Microporous Mesoporous Mater. 331 (2022) 111654, doi:10.1016/J.MICROMESO.2021.111654.
[48] R.M. Stephenson, S. Malanowski, Handbook of the thermodynamics of organic compounds, Handb. Thermodyn. Org. Compd. (1987), doi:10.1007/978-94-009-3173-2.
[49] R.L. Grob, E.F. Barry, in: Modern Practice of Gas Chromatography, 4th ed., Wiley, 2004, p. 1064. https://www.wiley.com/en-us/Modern+Practice+of+Gas+Chromatography%2C+4th+Edition-p-9780471229834.